

Energy Spectrum of the Electrons Accelerated by a Reconnection Electric Field: Exponential or Power Law?

W. J. Liu, P. F. Chen, M. D. Ding, and C. Fang

Department of Astronomy, Nanjing University, Nanjing 210093, China

chenpf@nju.edu.cn

ABSTRACT

The direct current (DC) electric field near the reconnection region has been proposed as an effective mechanism to accelerate protons and electrons in solar flares. A power-law energy spectrum was generally claimed in the simulations of electron acceleration by the reconnection electric field. However in most of the literature, the electric and magnetic fields were chosen independently. In this paper, we perform test-particle simulations of electron acceleration in a reconnecting magnetic field, where both the electric and magnetic fields are adopted from numerical simulations of the MHD equations. It is found that the accelerated electrons present a truncated power-law energy spectrum with an exponential tail at high energies, which is analogous to the case of diffusive shock acceleration. The influences of reconnection parameters on the spectral feature are also investigated, such as the longitudinal and transverse components of the magnetic field and the size of the current sheet. It is suggested that the DC electric field alone might not be able to reproduce the observed single or double power-law distributions.

Subject headings: Sun: flares — acceleration of particles—Sun: magnetic fields

1. INTRODUCTION

Particle acceleration remains a mystery in solar flares, as well as in cosmic rays from the extrasolar systems. Observationally, the energetic particles always show a single or double power-law spectral behavior. Three mechanisms have been proposed (see Miller et al. 1997; Aschwanden 2002, for reviews), i.e., the direct current (DC) electric field acceleration (e.g., Sturrock 1968), turbulence (or stochastic) acceleration (e.g., Miller 1998), and shock acceleration (e.g., Blandford & Ostriker 1978). Magnetic reconnection, as the effective mechanism

for magnetic energy release in solar flares, was demonstrated to be able to provide environments favorable for all the above-mentioned acceleration mechanisms to work (Chen et al. 2007).

DC electric field provides the simplest and most direct means of accelerating particles out of a thermal plasma (Holman 1985), which even allows for an analytical solution of each particle trajectory under certain assumptions (Bulanov 1980). In the case that the electric and magnetic fields induced by the accelerated particles are negligible, test particle simulations provide a simple and valid approach to study the particle acceleration in a reconnection-associated electric and magnetic fields. For example, Sakai (1992) showed that protons and electrons can be promptly accelerated (within 1 s) up to ~ 70 MeV and ~ 200 MeV, respectively. In order to compare the resulting energy spectrum of the DC-accelerated protons with observations, Mori, Sakai, & Zhao (1998) conducted test particle simulations with a hyperbolic magnetic field and a uniform electric field. The accelerated protons present a universal power-law spectrum, $f(E) \sim E^{-\delta}$, with the spectral index δ being $\sim 2.0 - 2.2$. Thereafter, a lot of test particle simulations have been performed for electrons as well, through either full orbit calculations (Zharkova & Gordovskyy 2004; Hamilton et al. 2005) or guiding center calculations (Wood & Neukirch 2005). Almost all of these simulations claimed to have obtained a power-law energy spectrum, with a spectral index around 2, similar to that for protons. It is noted, however, that the energy spectra in many of the published simulation results deviate significantly from a power-law profile. Moreover, according to the thick-target model, the resulting bremsstrahlung hard X-ray (HXR) emissions in these simulations would present a power-law energy spectrum with a spectral index around 1. However, the RHESSI observations indicated that the HXR emissions in most solar flares possess much softer spectra, with the spectral indices falling in the range between 3 and 7. As discussed by Chen et al. (2007), several factors may be attributed to such a big discrepancy. For example, the parameters of the reconnecting current sheet were chosen arbitrarily due to our poor knowledge of the physical conditions in the localized reconnection region in solar flares. Most importantly, the electric and magnetic fields, which should be coupled with each other through MHD equations, were often prescribed independently. Doing so often results in the electric and magnetic fields that are not compatible with the MHD equations. Some improvements were made in recent years. For example, Wood & Neukirch (2005) derived the electric field via the Ohm's law after assuming the distributions of the magnetic field, the velocity field, and the resistivity. A further progress was made by Hamilton et al. (2005), who deduced the solution of the linearized MHD equations by assuming that the longitudinal component of the magnetic field (B_z) and the velocity (\mathbf{v}) are small perturbations. In the real case, both B_z and \mathbf{v} can be quite large, therefore, it is necessary to obtain the electric and magnetic fields by directly solving the MHD equations.

In order to obtain self-consistent electric and magnetic fields, in this paper we first perform 2.5-dimensional MHD simulations of the resistive evolution of a current sheet. When a steady state is reached, the electric and magnetic fields are then taken out for test particle simulations. The paper is organized as follows. In §2, the numerical method is described, including the MHD and test particle simulations. The shape of the resulting energy spectrum is discussed in §3, and a parameter survey is conducted showing the influences of various parameters on the spectral features in §4. A short discussion is presented in §5.

2. PROBLEM SETUP AND NUMERICAL METHOD

2.1. Electric and Magnetic Field Configurations

In order to obtain self-consistent electric and magnetic fields, we numerically solve the following 2.5-dimensional (i.e., $\partial/\partial z = 0$), time-dependent, compressible resistive MHD equations with a multi-step implicit scheme (Hu 1989; Chen, Fang, & Hu 2000):

$$\frac{\partial \rho}{\partial t} + \nabla \cdot (\rho \mathbf{v}) = 0, \quad (1)$$

$$\frac{\partial \mathbf{v}}{\partial t} + (\mathbf{v} \cdot \nabla) \mathbf{v} + \frac{1}{\rho} \nabla P - \frac{1}{\rho} \mathbf{j} \times \mathbf{B} = 0, \quad (2)$$

$$\frac{\partial \psi}{\partial t} + \mathbf{v} \cdot \nabla \psi - \eta \Delta \psi = 0, \quad (3)$$

$$\frac{\partial B_z}{\partial t} + \mathbf{v} \cdot \nabla B_z + B_z \nabla \cdot \mathbf{v} - \mathbf{B} \cdot \nabla v_z - \nabla \cdot (\eta \nabla B_z) = 0, \quad (4)$$

$$\frac{\partial T}{\partial t} + \mathbf{v} \cdot \nabla T + (\gamma - 1) T \nabla \cdot \mathbf{v} - \frac{2(\gamma - 1)\eta}{\rho \beta_0} \mathbf{j} \cdot \mathbf{j} - CQ/\rho = 0, \quad (5)$$

where $\gamma = 5/3$ is the ratio of specific heats, η is the dimensionless resistivity, that is, the inverse of the magnetic Reynolds number. The last term on the left-hand side of equation (5) is the field-aligned heat conduction, where $Q = \nabla \cdot [T^{5/2}(\mathbf{B} \cdot \nabla T)\mathbf{B}/B^2]$, and C is the dimensionless coefficient (see Chen et al. 1999, for details). The five independent variables are the density (ρ), velocity (\mathbf{v}), magnetic flux function (ψ), the longitudinal component of the magnetic field (B_z), and temperature (T); note that the magnetic field \mathbf{B} is related to the magnetic flux function through $\mathbf{B} = \nabla \times (\psi \hat{\mathbf{e}}_z) + B_z \hat{\mathbf{e}}_z$. When nondimensionalizing the MHD equations, the characteristic density and temperature are fixed to be $\rho_0 = 1.67 \times 10^{-11}$ kg m⁻³ and $T_0 = 10^6$ K, respectively. While, the length scale (L_0) and the plasma beta (β_0) are free parameters. The velocity is normalized by the isothermal sound speed v_0 , and the

time is therefore by $\tau_0 = L_0/v_0$. Another time scale, the Alfvén transit time τ_A , is related to τ_0 by $\tau_A = \sqrt{\beta_0/2}\tau_0$. The dimensionless resistivity η is distributed as

$$\eta = \begin{cases} \eta_0 \cos(5\pi x) \cos[2(y-4)\pi], & \text{if } |x| \leq 0.1, |y-4| \leq 0.25, \\ 0, & \text{elsewhere,} \end{cases} \quad (6)$$

where η_0 is also a free parameter.

As the initial conditions, uniform density ($\rho = 1$) and temperature ($T = 1$) are assumed. The initial magnetic field is chosen to be a force-free field with a vertical current sheet located along the y -axis, which is written as

$$\psi = \begin{cases} (2w/\pi) \cos(\pi x/2w) - w & (|x| \leq w), \\ -|x| & (|x| > w), \end{cases} \quad (7)$$

$$B_z = \begin{cases} \sqrt{B_g^2 + \cos^2(\pi x/2w)} & (|x| \leq w), \\ B_g & (|x| > w), \end{cases} \quad (8)$$

where the half-width of the current sheet is $w = 0.1$, B_g is the longitudinal magnetic field (i.e., the guide component) in the background.

The dimensionless size of the simulation box is $-3 \leq x \leq 3$ and $0 \leq y \leq 8$. Because of the symmetry, the calculation is made only in the top right quadrant. The top ($y = 8$) and the right-hand ($x = 3$) sides are treated as open boundaries. Symmetry conditions are applied to the left-hand boundary ($x = 0$) and the bottom ($y = 4$) of the simulation quadrant. The detailed description of the MHD simulation can be found in Chen et al. (1999).

As the localized resistivity sets in, the elongated current sheet dissipates and collapses into an X-type magnetic configuration. After $\sim 7\tau_A$, the dynamics of the whole simulation region becomes steady, keeping all physical quantities almost invariant with time. Figure 1 shows the distributions of the temperature (*gray scale*), the magnetic field (*solid lines*), and the velocity (*vector arrows*) for the case with $B_g = 1$, $\beta_0 = 0.01$, and $\eta_0 = 0.02$ at $t = 8\tau_A$. Note that at the steady state, the z -component of the magnetic field near the reconnection X-point is around B_g . The small rectangular box in Figure 1 indicates the region where the resistivity does not vanish and where test particles are injected.

The corresponding electric field (\mathbf{E}) is then determined by the Ohm's law, i.e., $\mathbf{E} = \eta \nabla \times \mathbf{B} - \mathbf{v} \times \mathbf{B}$, where \mathbf{E} is nondimensionalized by the characteristic value of $v_0 B_0$, B_0 is the normalization unit of the magnetic field (see Chen et al. 1999, for details). Thereby,

the electric and magnetic fields are obtained for the ensuing test particle simulations. As an example, in the case of $\beta = 0.01$ and $\eta_0 = 0.01$, the electric field at the reconnection site is $\sim 600 \text{ V m}^{-1}$, which is super-Dreicer.

2.2. Test Particle Approach

Test electrons are uniformly distributed in the resistive region, which is indicated by the rectangle in Figure 1. Initially, these electrons have a Maxwellian velocity distribution with the local plasma temperature, which is superimposed on the local plasma bulk velocity. The motion of each electron is then calculated by numerically solving the following relativistic Lorentz equations

$$\frac{d}{dt}(\gamma m_0 \mathbf{v}) = q(\mathbf{E} + \mathbf{v} \times \mathbf{B}), \quad (9)$$

$$\frac{d\mathbf{x}}{dt} = \mathbf{v}, \quad (10)$$

where \mathbf{x} and \mathbf{v} are the particle position and velocity vectors, respectively; $\gamma = 1/\sqrt{1 - v^2/c^2}$ is the Lorentz factor, m_0 and q are the rest mass and the charge of the electron, respectively; \mathbf{E} and \mathbf{B} are the electric and magnetic fields obtained from the MHD simulations as described in the previous subsection. It is noted here that collisions are neglected in the momentum equation (9).

The 4th-order Runge-Kutta-Fehlberg (RKF45) scheme is used to solve the above equations, where the time step (Δt) is adaptive. In order to get smooth energy spectra, 2×10^5 test particles are simulated.

In order to confirm our test particle code, we repeated the simulations of proton acceleration that were performed by Mori, Sakai, & Zhao (1998), with the same electric and magnetic fields, i.e., $\mathbf{E} = (0, 0, E_z)$ and $\mathbf{B} = (\alpha y, \beta x, B_z)$. We chose the same parameters as in Mori, Sakai, & Zhao (1998) and found that the spectral indices are about 1.9-2.3, almost identical to their result, i.e., 2.0-2.2.

3. ENERGY SPECTRUM: POWER LAW OR EXPONENTIAL?

The electrons are accelerated under the action of the DC electric field promptly. At the same time, they gyro-rotate around the magnetic field lines. After certain rounds of

gyro-rotation, the accelerated electrons drift out of the resistive region, and then propagate away along magnetic separatrix layers between the reconnection inflow and outflow. Since the acceleration and the propagation of the electrons are 2-fold rotational symmetric, the particles going upward and downward are collected together to construct their energy spectrum. The left panel of Figure 2 plots the energy spectrum in a log-log scale for the case with $B_g = 1$, $L_0=100$ m, $\beta_0 = 0.01$, and $\eta_0 = 0.02$. To our surprise, the spectrum, which is quite smooth except for the high energy tail, does not show a single power-law profile (note that a single power-law profile is manifested as a linear line in the log-log scale). Apparently, it looks like a double power-law profile, as proposed in our recent review paper (Chen et al. 2007). The spectral profile is then fitted with a double power-law distribution, i.e., a harder power-law spectrum $f(E) \sim E^{-1.2}$ in the energy range of 2-40 keV (*red line*) plus a softer power-law spectrum $f(E) \sim E^{-3.9}$ in the energy range of 50-120 keV (*blue line*). It is noted that the spectral index at the high energy tail in our simulation is significantly higher than those obtained in the published test particle simulations, and is in the typical range of the electron spectral indices derived from HXR spectral observations.

The HXR observations from RHESSI did find double (or broken) power-law spectral profiles in some flares (e.g., Holman et al. 2003), and theoretical models have also been proposed to explain this feature (e.g., Zhang & Wang 2004). The profile in the left panel of Figure 2 is, however, somewhat different from the broken power-law distribution of Holman et al. (2003) in that the spectral profile changes gradually between the two power-law parts in our simulation results, while the transition is abrupt in the observation (Sui 2007).

In order to clarify the spectral distribution of the accelerated electrons in our simulations, we re-plot the energy spectrum in a linear-log scale in the right panel of Figure 2. It is seen that, except for the significantly enhanced lower energy tail, the spectral profile is almost a linear line in a wide energy range, which means that the spectrum is close to be exponential in most of the energy range. Considering the low energy tail, we fit the spectral profile with the combination of an exponential and a power-law functions, i.e., $f(E) \sim E^{-\delta}e^{-E/E_0}$. With the spectral index $\delta = 0.35$ and the rollover energy $E_0=23.1$ keV, the fitted line (*pink*), as shown in the right panel of Figure 2, is consistent with the simulation result in most of the energy range, from 8 to over 120 keV.

Although it was claimed by many authors that DC electric field in magnetic reconnection leads to a power-law energy spectrum of the accelerated electrons, quite often the spectrum obtained from test particle simulations deviates significantly from a perfect power-law distribution. Several authors already noted that the energy spectrum of the DC-accelerated electrons may be characterized as either power-law or exponential, depending on the value of B_z (Hamilton et al. 2005) or the trapping time of the electrons inside the acceleration vol-

ume (Anastasiadis, Vlahos, & Georgoulis 1997). The test particle simulations in this paper, with self-consistent electric and magnetic fields obtained from MHD simulations, indicate that the electrons accelerated by the DC electric field of magnetic reconnection present a spectrum with the form

$$f(E) \sim E^{-\delta} e^{-E/E_0}, \quad (11)$$

which is similar to those obtained in the diffusive shock acceleration when the power-law behavior is truncated by a variety of effects (see Ellison & Ramaty 1985, for discussions). The same spectral profile was also obtained in the electron acceleration by random DC electric field (Anastasiadis et al. 2002). It is, however, mentioned here that among all our simulated scenarios, only in one case with $B_g = 1.0$, $L_0=50$ m, $\beta_0 = 0.01$, and $\eta_0 = 0.005$, the energy spectrum does show a clear broken power-law shape.

4. PARAMETER SURVEY

Several parameters can affect the energy spectral profile of the DC-accelerated electrons in our simulations, where the spectral profile is characterized by δ and E_0 as indicated by equation (11). The free parameters include the longitudinal component of the magnetic field (B_g), the length scale (L_0), the resistivity (η_0), and the magnetic field strength, as represented by the plasma beta (β_0). In the following subsections, the effect of varying each parameter is investigated individually with other parameters keeping fixed.

4.1. Effect of the Guide Field B_g

By theoretical analysis of electron acceleration in a reconnecting current sheet, Litvinenko (1996) propounded that a longitudinal component of magnetic field is necessary to explain the accelerated electrons with energy up to 100 keV. In our simulations, the longitudinal component (i.e., the guide component along the z -direction) of the magnetic field near the reconnection X-point is around B_g . Therefore, we calculated six cases with B_g increasing from 0 to 1.0, while the other parameters are $L_0=50$ m, $\beta_0 = 0.01$, and $\eta_0 = 0.02$. The energy spectra of the accelerated electrons in the six cases are depicted in the upper panel of Figure 3. It is clear that, as B_g increases, more and more electrons are accelerated to high energies, which confirms the importance of longitudinal magnetic field in accelerating electrons to higher energies (Litvinenko 1996). The dependence of δ and E_0 on B_g is plotted in the lower panel of Figure 3. It is found that as B_g increases, E_0 increases steadily, while

δ first falls rapidly when B_g increases from 0 to 0.4, and then increases slowly.

In order to study the efficiency of DC acceleration, we calculate the percentage of electrons whose energy is higher than 10 keV, and define it as the acceleration rate. We find that when B_g is zero, few particles are accelerated and the acceleration rate is 0.0475%. However, when B_g reaches 1, the acceleration rate jumps to 11.3%.

4.2. Effect of the Length Scale L_0

The size of the current sheet is an important but unknown parameter in the flaring process. Therefore, it is worth studying how this parameter would affect the energy spectrum of the electrons. As shown in Figure 1, the initial size of the reconnection sheet is $0.2L_0 \times 0.5L_0$, where L_0 is the length scale of the MHD simulations. With $B_g = 1$, $\beta_0 = 0.005$, and $\eta_0 = 0.02$ being fixed, test particle simulations are conducted in four cases with L_0 being 10, 50, 100, and 200 m, respectively. The upper panel of Figure 4 shows the energy spectra of the accelerated electrons in the four cases. It is seen that as L_0 increases, more and more electrons are accelerated to high energies. This is easy to understand since as L_0 increases, electrons travel a longer distance in the electric field before they migrate out of the acceleration region due to gyration. The dependencies of δ and E_0 on L_0 are shown in the lower panel of Figure 4. It is seen that E_0 increases almost linearly with L_0 , while δ initially increases rapidly with L_0 , and then saturates after $L_0=100$ m. We calculated the fraction of the electrons with energies exceeding 10 keV, and found that the acceleration rate increases from 4.49% to 26.3% as L_0 increases from 10 to 200 m.

4.3. Effect of the Plasma beta β_0

In the Petschek model for magnetic reconnection (Petschek 1964), the electric field near the reconnection X-point is proportional to B_0^2 , where B_0 is the magnetic field strength in the inflow region. Therefore, the spectral shape of the accelerated electrons should be sensitive to the magnetic field. Here, the magnetic field (B_0) is characterized by the plasma beta, i.e., $\beta_0 = 2\mu_0\rho_0RT_0/B_0^2$. With the choice of ρ_0 and T_0 as in §2, B_0 is related to β_0 by $B_0 \sim 7/\sqrt{\beta_0}$ in units of gauss. With $B_g = 1$, $L_0=50$ m, and $\eta_0 = 0.02$, we simulated four cases with different β_0 . The upper panel of Figure 5 shows the energy spectra of the accelerated electrons in the four cases. As expected, it is seen that as β_0 decreases, i.e., the magnetic field increases, more electrons are accelerated to high energies, and the spectrum at the high energy tail tends to become harder. The dependence of δ and E_0 on β_0 is plotted

in the lower panel of Figure 5, which shows that as β_0 decreases, E_0 increases significantly, while δ increases when β_0 decreases from 0.1 to 0.01 and then decreases. The acceleration rate increases significantly from 0.169% to 15.2% as β_0 decreases from 0.1 to 0.005.

4.4. Effect of the Resistivity η_0

The resistivity in a reconnecting current sheet is caused by the local microscopic instability of plasma and it is still an unknown parameter in the flaring process. In our simulations the resistivity is characterized by the free parameter η_0 . With $B_z = 1$, $\beta_0 = 0.01$, and $L_0 = 50$ m, five cases with different η_0 are simulated. Note that $\eta_0 = 0.01$ corresponds to an anomalous magnetic diffusivity of $7 \times 10^4 \Omega \text{ m}$, $\sim 10^5$ times the classic value, which is quite similar to the numerical results of particle-in-cell simulations (Petkaki et al. 2003; Karlický & Bárta 2008). Such an anomalous magnetic diffusivity, in addition to the small normalization length scale, makes the magnetic Reynolds number, i.e., the inverse of η_0 , be ~ 100 . The upper panel of Figure 6 shows the corresponding energy spectra of the accelerated electrons. It is found that the acceleration rate slightly increases from 10.1% to 11.3% as η_0 increases from 0.005 to 0.02 and then slightly decreases to 9.70% as η_0 increases to 0.08. The weak dependence of the acceleration rate is actually due to the population decrease of the electrons above ~ 20 keV and the population increase of the electrons between ~ 10 keV and ~ 20 keV as η_0 increases. The dependence of δ and E_0 on η_0 is depicted in the lower panel of Figure 6. It is seen that both δ and E_0 decreases with the increase of η_0 .

5. DISCUSSION

X-ray and γ -ray observations of solar flares indicated that electrons and protons are instantly accelerated in the magnetic reconnection process. Analyses of HXR spectral data revealed that the accelerated electrons present a single power-law energy spectrum in most flares or a double power-law spectrum in some other events. The co-existence of normal and reverse type III radio bursts strongly suggests that nonthermal electrons are accelerated near the reconnection X-point within a compact region less than 2000 km in length (Aschwanden 2002). Near the reconnection X-point, both DC electric field and the reconnection-associated turbulence may contribute to the acceleration of these nonthermal electrons (Sturrock 1968; Chen et al. 2007). The DC mechanism, as the simplest model, has been studied by various groups with help of test particle simulations. Although the resulting energy spectrum of the accelerated electrons is somewhat power law-like, the spectral indices seem to be much smaller than the typical values derived from HXR observations. Therefore, more work is

required to fill the gap between test-particle simulations and observations.

Using self-consistent electric and magnetic fields obtained from numerical simulations of 2.5-dimensional nonlinear MHD equations, we investigated the energy spectrum of the electrons that are accelerated by the DC electric field in a reconnecting current sheet. Contrary to many of the previous studies, our test particle simulations indicate that the accelerated electrons present a power-law spectrum truncated by an exponential high energy tail, i.e., $f(E) \sim E^{-\delta} e^{-E/E_0}$, which is similar to the case of diffusive shock acceleration (Ellison & Ramaty 1985) and the case of random DC-electric field acceleration when the electron trapping time is long (Anastasiadis, Vlahos, & Georgoulis 1997). A parameter survey is conducted to investigate how various physical quantities affect the spectral profile and the acceleration rate. As the energy spectra are fitted with the function $f(E) \sim E^{-\delta} e^{-E/E_0}$, it is found that

(1) E_0 , the rollover energy, increases with larger B_g (the guide magnetic field), larger L_0 (which characterizes the size of the reconnection diffusion region), smaller β_0 (the plasma beta), and smaller η_0 (the resistivity);

(2) δ increases with larger L_0 and smaller η_0 , and it saturates as L_0 is larger than 100 m or η_0 is very small. The dependence of δ on B_g or β_0 is not monotonic. δ reaches the minimum when B_g is ~ 0.4 times the antiparallel component of the reconnecting magnetic field, while δ reaches the maximum when β_0 is around 0.01;

(3) The acceleration rate, defined here as the percentage of the electrons that are accelerated above to 10 keV, increases with larger B_g , larger L_0 , and smaller β_0 . It does not change much with η_0 , although the percentage of the electrons above 20 keV steadily decreases with increasing η_0 .

The truncated power-law energy spectrum obtained in this paper is somewhat similar to the double power-law distribution, although the transition between the low and high energy tails is not so abrupt in most cases. The research in this paper reveals that, even with self-consistent electric and magnetic fields, we still cannot reproduce the observed single or double power-law energy spectra of the nonthermal electrons in the framework of DC-electric field mechanism. This discrepancy between test particle simulations and observations might be reconciled if other effects are included. For example, the turbulence in the reconnection site would greatly enhance the collision rate between nonthermal electrons and background particles or waves (Wu et al. 2005). In other words, DC-electric field in the reconnection site alone may not be able to explain the observed spectral features of nonthermal electrons. The combination of DC-electric field and the turbulence may finally lead to single or double power-law spectral distributions, which were derived from HXR observations. This is

definitely an issue requiring further investigation.

One of the authors (WJL) thanks V. V. Zharkova and Y. Dai for their helpful discussions and suggestions. This research is supported by the Chinese foundations GYHY200706013, FANEDD (200226), 2006CB806302, NSFC (10221001, 10403003, and 10673004).

REFERENCES

- Anastasiadis, A., Vlahos, L., & Georgoulis, M. K. 1997, *ApJ*, 489, 367
- Anastasiadis, A., Gontikakis, C., Vilmer, N., & Vlahos, L. 2002, *Proc. of the Magnetic Coupling of the Solar Atmosphere Euroconference*, 505, 337
- Aschwanden, M. J. 2002, *Space Sci. Rev.*, 101, 1
- Blandford, R. D., & Ostriker, J. P. 1978, *ApJ*, 221, L29
- Bulanov, S. V. 1980, *Sov. Astron. Lett.*, 6, 206
- Chen, P. F., Fang, C., & Hu, Y. Q. 2000, *Chin. Sci. Bull.*, 45, 798
- Chen, P. F., Fang, C., Tang, Y. H., & Ding, M. D. 1999, *ApJ*, 513, 516
- Chen, P. F., Liu, W. J., & Fang, C. 2007, *Adv. Space Res.*, 39, 1421
- Ellison D. C., & Ramaty R. 1985, *ApJ*, 298, 400
- Hamilton, B., Fletcher, L., McClements, K. G., & Thyagaraja, A. 2005, *ApJ*, 625, 496
- Holman, G. D. 1985, *ApJ*. 293, 584
- Holman, G. D., Sui, L., Schwartz, R. A., & Emslie, A. G. 2003, *ApJ*, 595, L97
- Hu, Y. Q. 1989, *J. Comput. Phys.*, 84, 441
- Karlický, M., & Bárta, M. 2008, *Sol. Phys.*, 247, 335
- Litvinenko, Y. 1996, *ApJ*, 462, 997
- Miller, J. A., Cargill, P. J., Emslie, A. et al. 1997, *JGR*, 102, 14631
- Miller, J. A. 1998, *Sol. Phys.*, 86, 79
- Mori, K., Sakai, J., & Zhao, J. 1998, *ApJ*, 494, 430

- Petkaki, P., Watt, C. E. J., Horne, R. B., & Freeman, M. P. 2003, *Journal of Geophysical Research (Space Physics)*, 108, 1442
- Petschek, H. E. 1964, in *The Physics of Solar Flares*, ed. W. N. Hess (NASA SP-50; Washington, DC: NASA), 425
- Sakai, J.-I. 1992, *Sol. Phys.*, 140, 99
- Sturrock, P. A. 1968, *IAU Symp.*, 35, 471
- Sui, L. H. 2007, private communications
- Wood, P., & Neukirch T. 2005, *Sol. Phys.* 226, 73
- Wu, G.-P., Huang, G.-L., & Tang, Y.-H. 2005, *Chin. J. Astron. Astrophys.*, 5, 99
- Zharkova, V. V., & Gordovskyy, M. 2004, *ApJ*, 604, 884
- Zhang T. X., & Wang J. X. 2004, *ApJ*, 613, L165

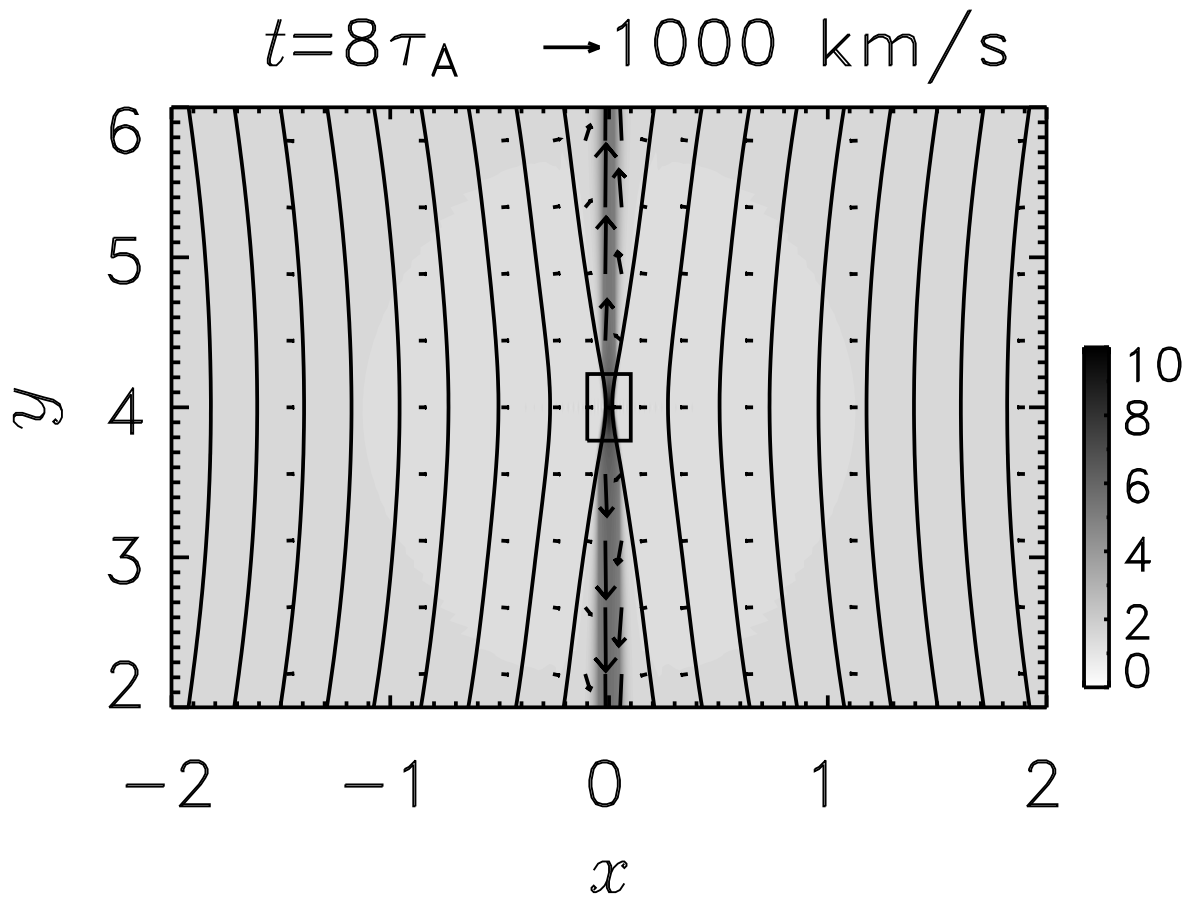


Fig. 1.— Distributions of the temperature (*gray scale*), the magnetic field (*solid lines*), and the velocity (*vector arrows*) at $t = 8\tau_A$. The rectangle around the reconnection X-point is the site where test particles are injected.

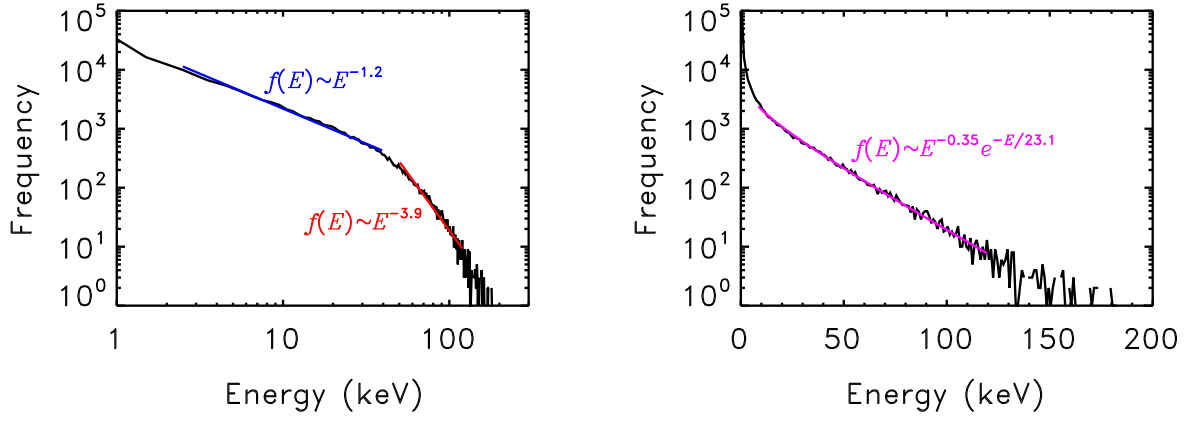


Fig. 2.— Energy spectrum of the nonthermal electrons for the case with $B_z = 1$, $L_0 = 100$ m, $\beta_0 = 0.01$, and $\eta_0 = 0.02$ plotted in a log-log scale (*left*, which is fitted with a double power law) and a linear-log scale (*right*, which is fitted with a power law truncated by an exponential tail).

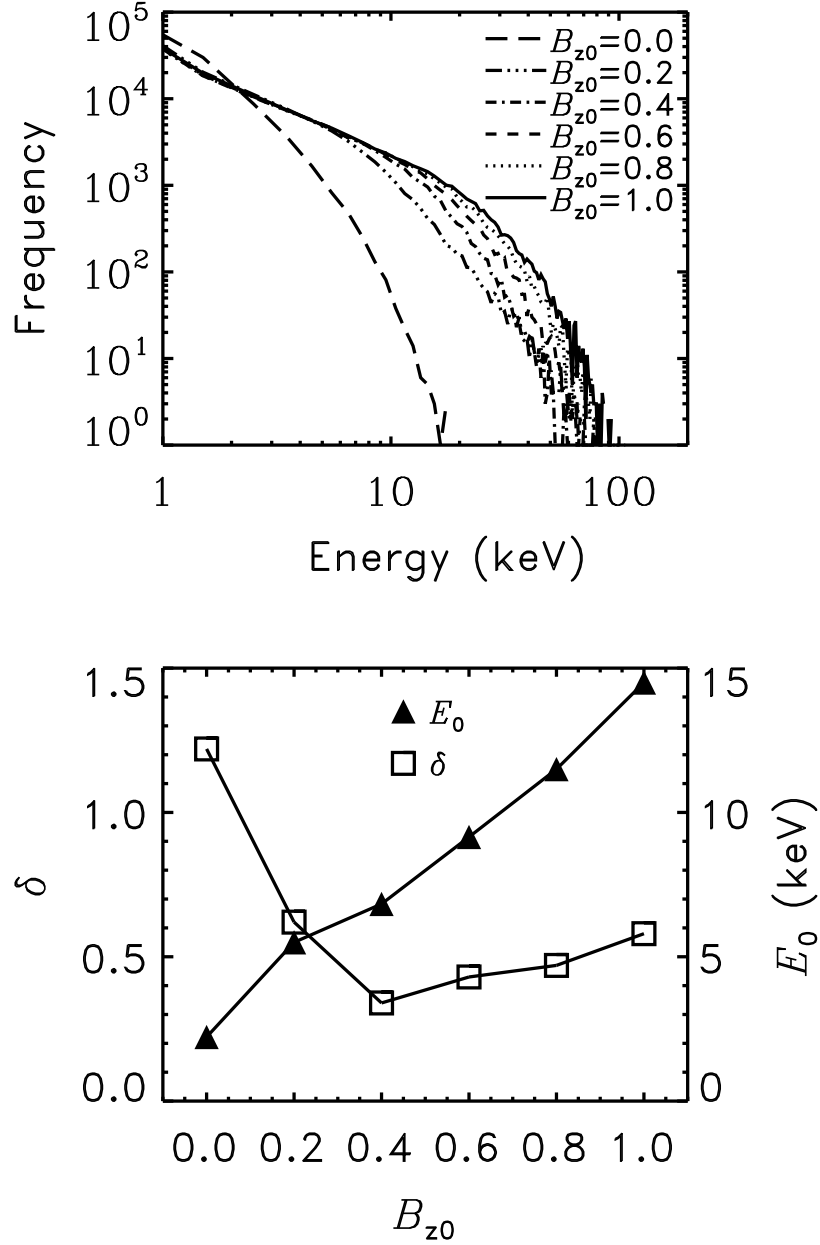


Fig. 3.— *Upper*: Energy spectra of the nonthermal electrons in six cases with different guide magnetic field B_g , where other parameters are fixed ($L_0=50$ m, $\beta_0 = 0.01$, and $\eta_0 = 0.02$). *Lower*: Variations of δ and E_0 with B_g .

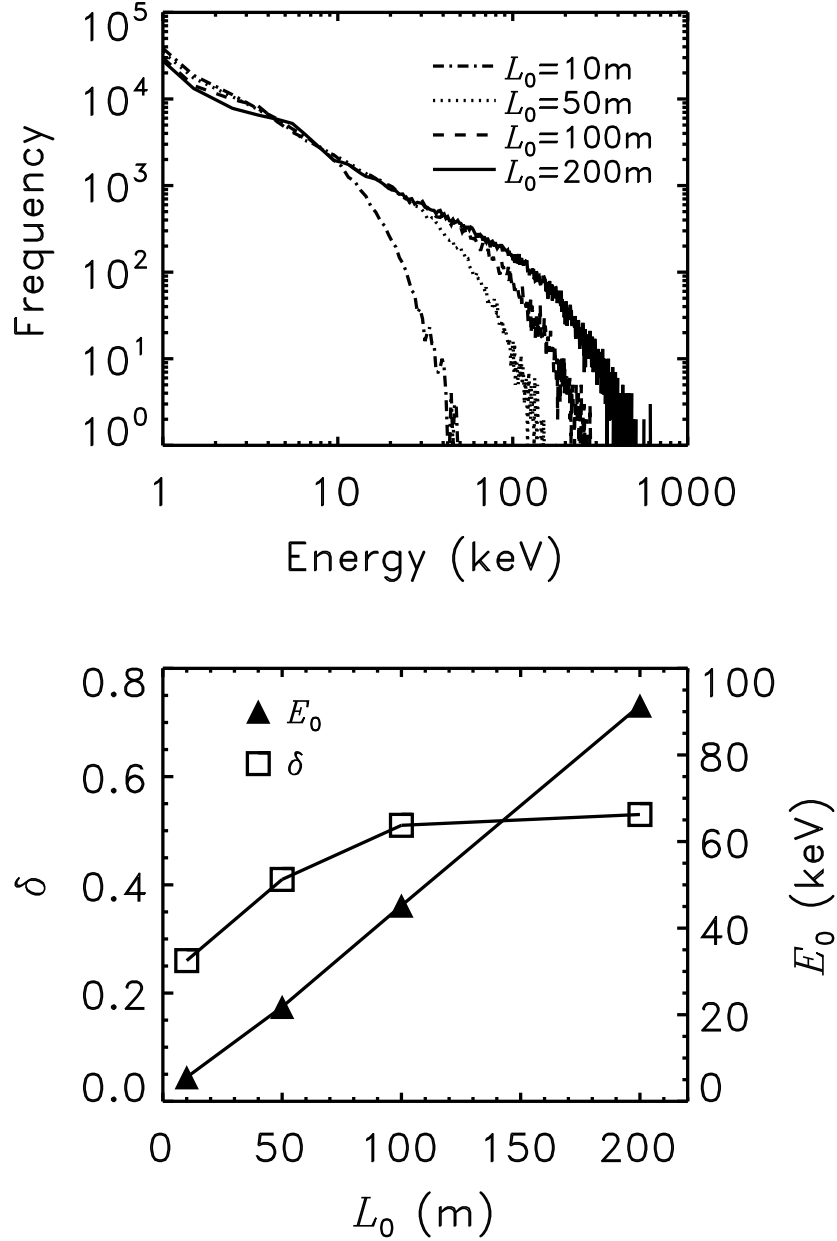


Fig. 4.— *Upper*: Energy spectra of the nonthermal electrons in four cases with different length scale L_0 , where other parameters are fixed ($B_g = 1$, $\beta_0 = 0.005$, and $\eta_0 = 0.02$). *Lower*: Variations of δ and E_0 with L_0 .

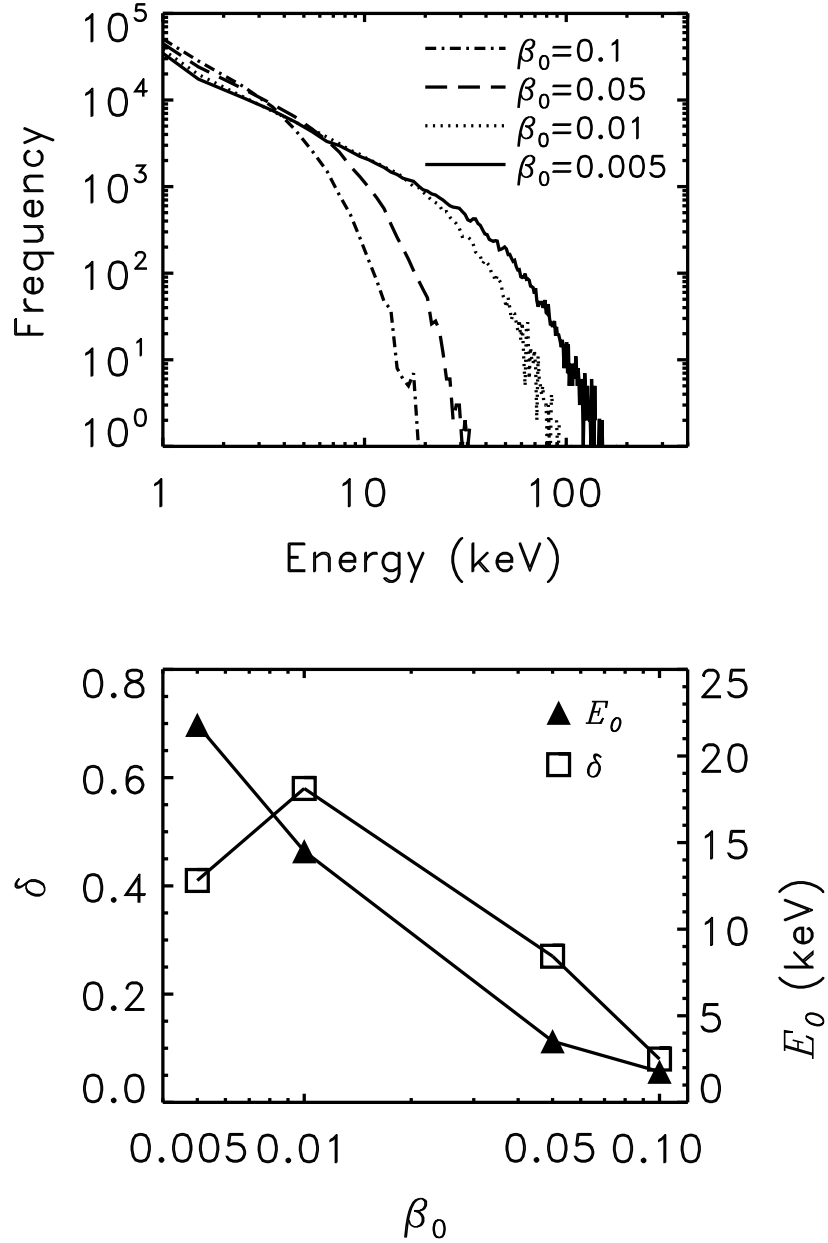


Fig. 5.— *Upper*: Energy spectra of the nonthermal electrons in four cases with different β_0 , where other parameters are fixed ($B_g = 1$, $L_0 = 50$ m, and $\eta_0 = 0.02$). *Lower*: Variations of δ and E_0 with β_0 .

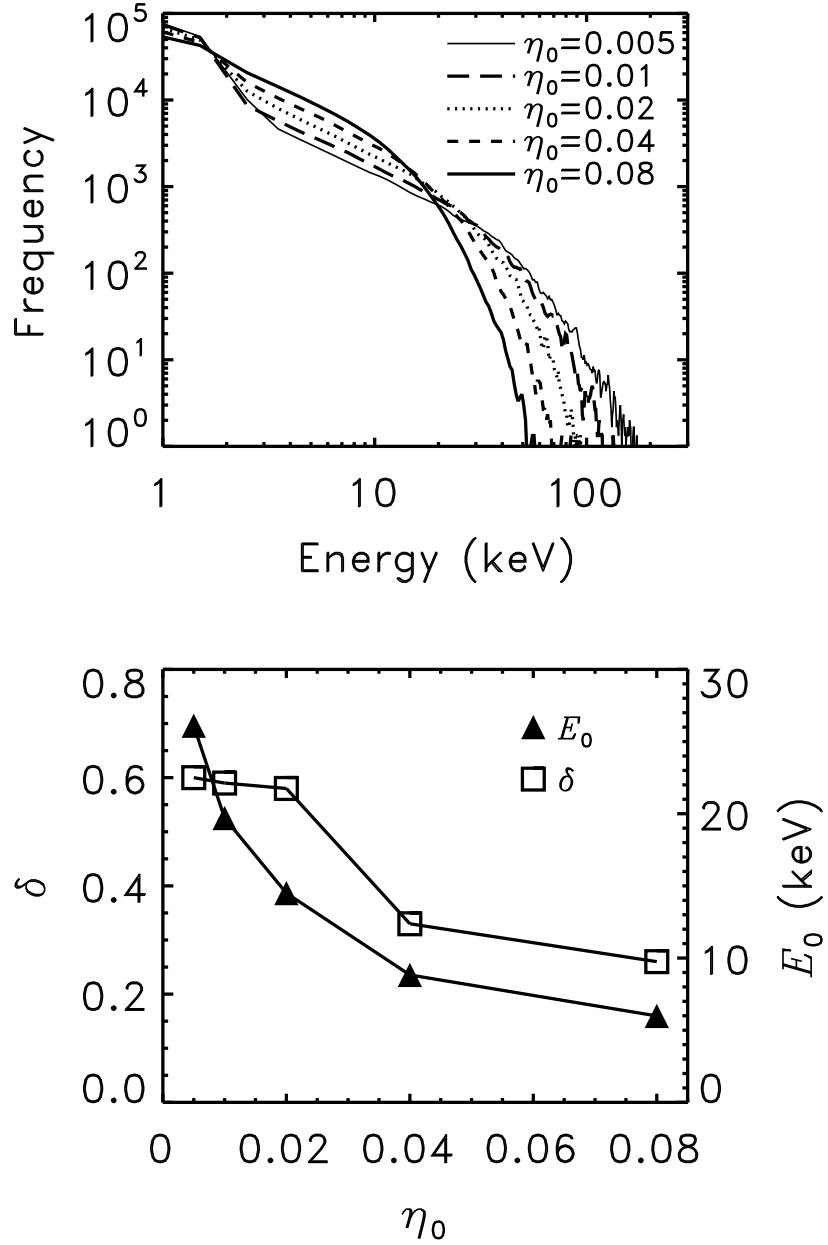


Fig. 6.— *Upper*: Energy spectra of the nonthermal electrons in four cases with different η_0 , where other parameters are fixed ($B_g = 1$, $L_0 = 50$ m, and $\beta_0 = 0.01$). *Lower*: Variations of δ and E_0 with η_0 .